Modification of antiphase domain sizes in omphacite by dislocation glide and creep mechanisms and its petrological consequences

H. L. M. VAN ROERMUND* AND J. M. LARDEAUX

Ecole Normale Supérieure de Lyon, Lab. des Sciences de la Terre, 46 Allée d'Italie, 69364 Lyon Cedex 07, France

Abstract

A T.E.M. study of omphacites from the western Italian Alps (Sesia Lanzo Zone and Monviso eclogites) has revealed a bimodal size distribution of antiphase domains: (*a*) 250–350 Å, (*b*) ≥ 2500 Å. In addition observed dislocation substructures and 'large-scale' antiphase domains are intimately interconnected.

A model is presented that can explain modification of the antiphase domain sizes by the interplay of cooling/growth and dislocation glide and/or creep mechanisms. Subsequent coarsening of the modified antiphase domains is inferred to be the result of surface free-energy processes. The model clearly illustrates that only the 'relatively undeformed' areas containing the small-scale antiphase domains can be used for thermometric methods.

KEYWORDS: western Italian Alps, omphacite, antiphase domain, 1/2<110> dislocation.

Introduction

ONE of the aims of metamorphic petrology is to determine the evolution of the physical conditions which prevailed in orogenic terrains. In the domain of high-pressure metamorphism (blueschists and eclogites) a thermometric method has been proposed by Carpenter (1981*a*,*b*). This method is based on the coarsening behaviour of antiphase domains (APDs) in omphacite, which are formed due to an order/disorder phase transformation (Champness, 1973; Phakey and Ghose, 1973).

Carpenter (1981*a*,*b*) proposed the following relationship between APD size (Å), temperature (T, °K) and annealing time (t, years) for omphacites:

$$(\text{APD size})^8 = 8 \times 6 \times 10^{35} \exp.\ (-75000/RT)t.$$

The equation parameters were derived experimentally, while the form of the equation is equivalent to the known coarsening behaviour of APDs in metals.

This thermometric method, which is sensitive at temperatures below 650 °C to the peak metamorphic temperature (T) rather than the isothermal time (t) or the cooling stage parameters (Carpenter, 1981*a*; Nisio, 1985), yields results which are consistent with that of more 'classical' thermometers in eclogites such as the cationic (Fe, Mg) exchange reactions between garnet, clinopyroxene, orthopyroxene and phengite (Råheim and Green, 1975; Ellis and Green, 1979; Carswell *et al.*, 1985; Lardeaux *et al.*, 1986).

However, results obtained by Carpenter (1981*a* and Fig. 1) on APD sizes in omphacites from the western Italian Alps (Sesia Zone) are inconsistent with other available data obtained by conventional methods such as mineral assemblages, thermometrical calculations and geological data. This discrepancy arises from the large APD sizes (≥2500 Å) reported by Carpenter (1981*a*) in omphacites from the Sesia Lanzo Zone, despite the moderate peak metamorphic conditions under which they formed. However, our transmission electron microscopy (T.E.M.) investigations on omphacites from two different metamorphic terrains in the western Italian Alps (Monviso and Sesia Lanzo Zone eclogites) have elucidated a bimodal APD size distribution in omphacites from both areas. In both areas the

* Present address: Laboratoire de Pétrologie Métamorphique, C.N.R.S., URA 736, Université de Paris 7, 4 Place Jussieu, F-75252 Paris Cedex 05, France.

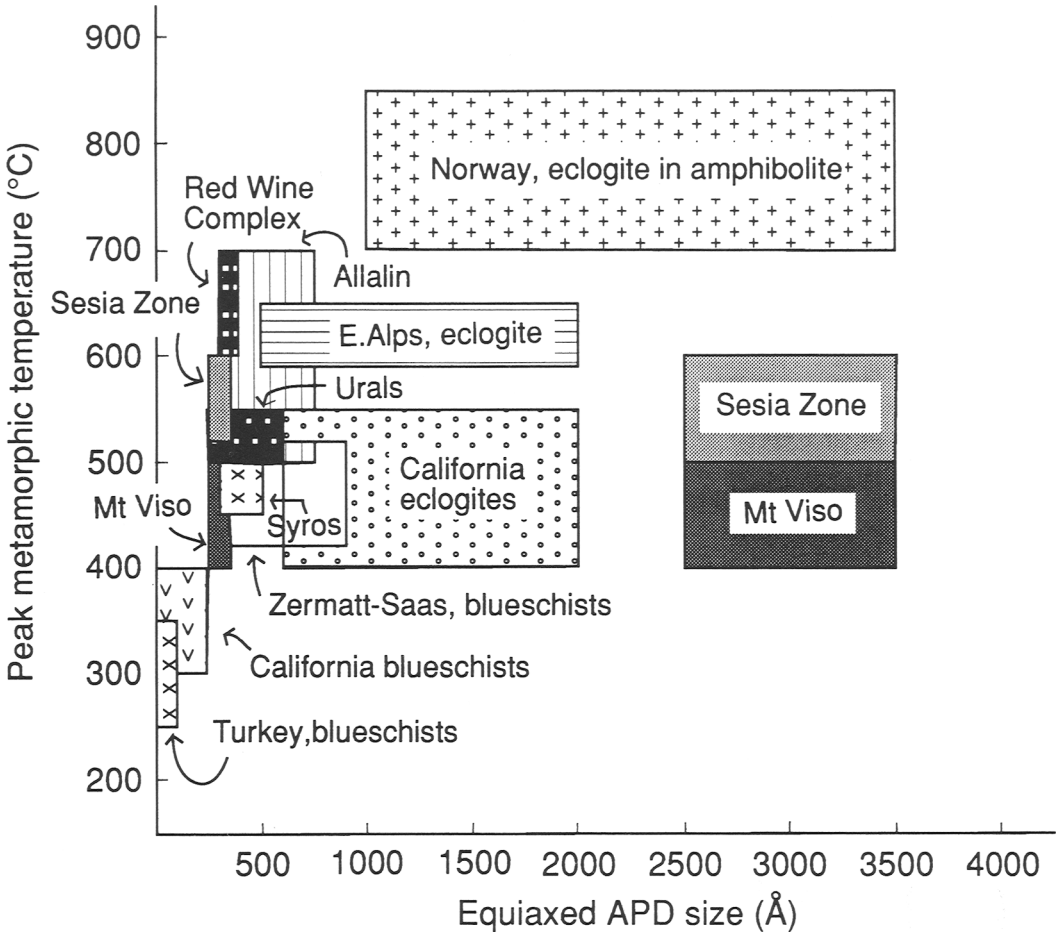

FIG. 1. Temperature versus APD size diagram. Modified after Carpenter (1981*a*). Note: for Sesia Zone Carpenter reports only APD sizes ≥2500 Å.

smaller APD sizes are consistent with Carpenter's (1981*a*) predictions.

Earlier workers have interpreted a bimodal APD size distribution in terms of different nucleation mechanisms, viz. homogeneous versus heterogeneous nucleation (along pre-existing defects), or by homogeneous versus heterogeneous coarsening mechanisms (see Buseck *et al.*, 1980, and references therein).

The purpose of the present contribution is to examine whether the bimodal APD size distribution in omphacites can be explained by the interaction of APD coarsening and intracrystalline deformation mechanisms.

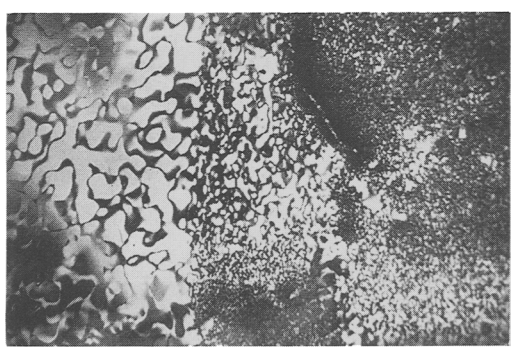

FIG. 2. Electron micrograph showing the observed range in APD sizes in omphacite from Monviso. Bottom left side: ≥2500 Å; right side 250–350 Å.

Geological context and sample description

For a detailed geological description of the Monviso eclogites the reader is referred to Dal

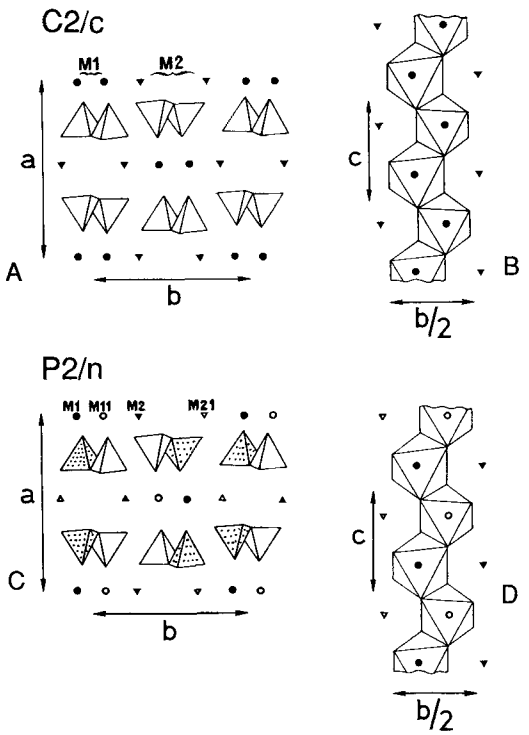

FIG. 3. (A) Schematic view of disordered *C2/c* omphacite in the (001) plane. (B) The M_1 octahedral strip in *C2/c* omphacite. (C) Schematic view of ordered *P2/n* omphacite in the (001) plane. (D) The M_1 octahedral strip in *P2/n* omphacite.

Piaz (1974); Caby *et al.* (1978); Lombardo *et al.* (1978); Nisio (1985); Nisio *et al.* (1987) and Philippot (1988 and 1990) and for the Sesia Lanzo Zone eclogites to Compagnoni *et al.* (1977); Lardeaux *et al.* (1982); Vuichard (1989) and Lardeaux and Spalla (1991).

Temperature estimates are 450 ± 50 °C for Monviso eclogites (Kienast, 1983; Lardeaux *et al.*, 1986) and 500–600 °C for the Sesia Lanzo Zone (Compagnoni *et al.*, 1977; Koons, 1982; Lardeaux *et al.*, 1982 and Vuichard and Ballèvre, 1986). In both cases detailed field studies and optical observations on omphacites demonstrated deformation-induced recrystallisation microstructures such as undulatory extinction, subgrains and recrystallised new grains. Associated dislocation substructures have been described by Nisio (1985), Buatier and Lardeaux (1987) and Buatier *et al.* (1991). The dislocation substructures consist of isolated [001] and 1/2<110> dislocations, dissociated 1/2<110> dislocations, nodal points, tiltwalls, complex dislocation networks and (010) planar defects. We have verified, except for the (010) planar defects, all above-mentioned defects by electron diffraction experiments. Our results were identical. However, we have not made a detailed study of the (010) planar defects, and their nature remains to be resolved. In addition, APD sizes measured by us and repeated by others show a bimodal distribution of small (250–350 Å) and large (≥ 2500 Å) APDs for both metamorphic terrains (Carpenter, 1981; Nisio, 1985; Fig. 2). Because of the intimate intergrowth of dislocation substructures with the larger APD sizes, Nisio (1985) and Lardeaux *et al.* (1986) suggested a modification of the APD size distribution by deformation. However the details of the mechanism remained to be resolved.

Crystal structure

Before we go into the details of omphacite deformation mechanisms, a short description of the crystal structure of *C2/c* and *P2/n* clinopyroxenes will be useful. *C2/c* omphacite can be described as an alternating sequence of tetrahedral and octahedral layers parallel to (100) (Fig. 3). The tetrahedral layer is built up by chains of Si–O tetrahedra parallel to [001]. The layer improperly called octahedral contains zig-zag

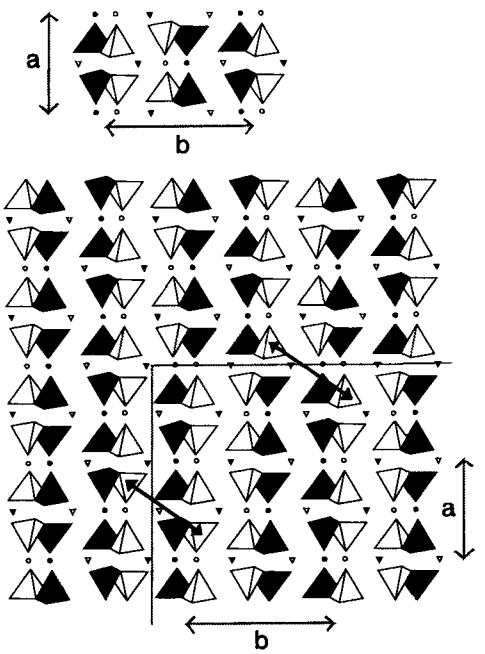

FIG. 4. Model of an APD boundary in *P2/n* omphacite. The displacement vector (R = 1/2<110>) is indicated by the arrow. Note: there is no control on cation positions in the APD boundary.

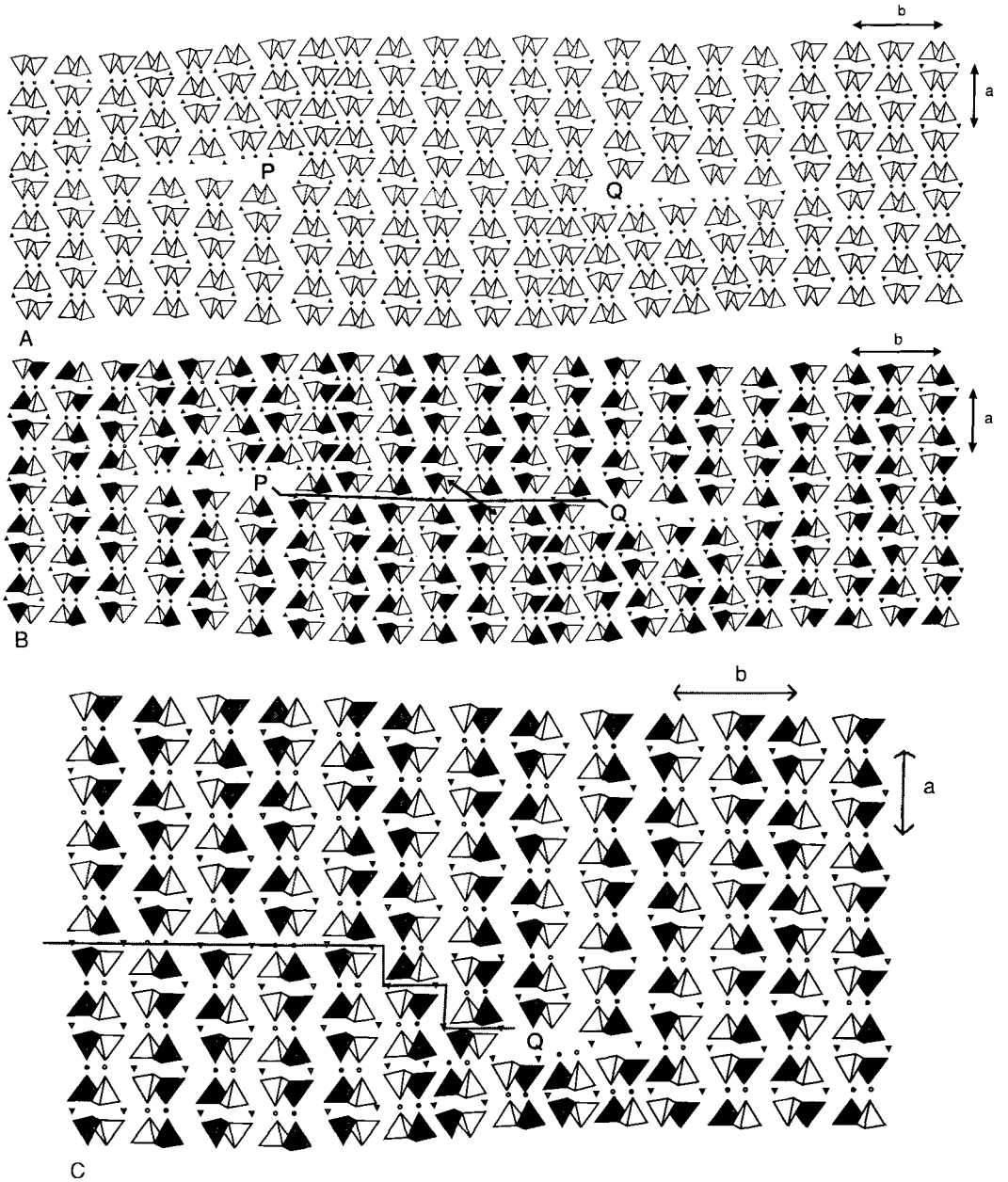

FIG. 5 (A) Model of a simple dipole (two 1/2<110> edge dislocations labelled P and Q respectively) in the *C2/c* omphacite structure. Projection parallel to (001). Note extra half planes parallel to (100) and (010). (B) Model of identical dipole as in Fig. 5A in the *P2/n* crystal structure. Note fault (crystallographic shear plane) connecting both partial dislocations P and Q. The displacement vector across the fault is 1/2<110> and is indicated by the arrow. (C) Dislocation Q (Fig. 5B) has slipped along (110) dragging the fault behind it.

chains of M_1 octahedra and M_2 eight-coordinated cations. The chemical formula of omphacite is $M_2M_1T_2O_6$ with T = Si; M_1 = Mg, Al, Fe^{2+}, (Fe^{3+}), (Cr), (Ti), and M_2 = Ca, Na, (Fe^{2+}). In the high-temperature *C2/c* polymorph the distribution of the M_1 and M_2 cations is homogeneous giving rise to identical tetrahedral chains and identical M_1/M_2 chains (parallel to [001]) in the

C-centred unit cell (Fig. 3A and B). However in the low-temperature *P2/n* polymorph the M_1 and M_2 cations are systematically ordered, giving rise to two distinct adjoining Si–O tetrahedra in the primitive unit cell (Fig. 3C and D). For more elaborate information on the crystal–chemical structure of omphacite the reader is referred to Rossi (1988). Note also that the degree of ordering in omphacite is a function of composition and possibly of temperature (Rossi *et al.*, 1983; Kienast *et al.*, 1991).

Due to the ordering of M_1 and M_2 cations and the distinct Si–O tetrahedra, APDs can be produced in the low-temperature *P2/n* structure (Fig. 4). The displacement vector along an antiphase domain boundary is 1/2<110> (Champness, 1973; Phakey and Ghose, 1973). APD production arises during the polymorphic phase transformation of 'high-temperature' *C2/c* to 'low-temperature' *P2/n* crystal structures. Also in the case of omphacite growth directly in the *P2/n* stability field, metastable growth of *C2/c* omphacite predates cationic ordering processes (Champness, 1973).

Deformation mechanisms

Depending on which physical parameters (confining pressure, deviatoric stress, strain rate, temperature, impurity contents) are operating, clinopyroxene microstructures reveal a wide range of deformation mechanisms ranging from brittle, brittle–ductile to completely ductile deformation and recrystallisation (Avé-Lallement, 1978; Van Roermund and Boland, 1981; Van Roermund, 1984; Kirby and Kronenberg, 1984; Boland and Tullis, 1986 and Buatier *et al.*, 1991). Within the plastic-deformation field the following slip systems have been reported: (100)[001]; {110}[001] and 1/2<110>{110}. In addition, Ratterson and Jaoul (1991) and Ingrin *et al.* (1991) have demonstrated that at elevated temperatures the influence of the (100)[001] slip system becomes limited. Therefore a combination of these slip systems, aided by climb processes, enables clinopyroxenes to deform plastically. In addition, a third geometrically necessary dislocation with Buergers vector 1/2<112> is observed in complex dislocation networks, defined by triple point junctions, allowing the generation of the dislocation reaction [001] + 1/2<110> − >1/2<112> (Van Roermund and Boland, 1981).

Modification of APD sizes can only be produced by dislocation glide and/or creep processes if the size and direction of the displacement vector (R) of the APBs and dislocations are identical. For this reason we will restrict ourselves to the 1/2<110>{110} slip system (Fig. 4). It is important, however, to realise that all high-temperature deformation studies have been performed on *C2/c* clinopyroxenes. However, the common 1/2<110> dislocation is a perfect dislocation in high-temperature *C2/c* clinopyroxenes, but becomes imperfect (or partial) in low-temperature *P2/n* crystal structures where, for instance, stacking faults are associated with the gliding 1/2<110> dislocations and complex faults with climbing 1/2<110> dislocations. Some natural examples of imperfect 1/2<110> dislocations in *P2/n* omphacite are given by Buatier *et al.*,

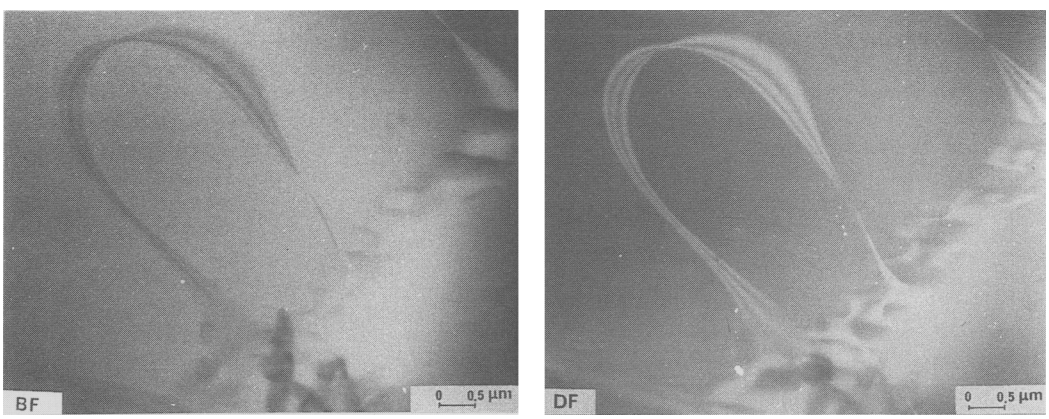

FIG. 6. Bright and dark field electron micrographs (g = 101) illustrating the interaction between APD boundaries and a (110) tiltwall in *P2/n* omphacite. Note (1) APD boundaries end at dislocations, (2) stacking faults connect two adjacent partial 1/2<110> dislocations, (3) identical fringe patterns in bright and dark field modes for both type of faults, and (4) all defects are invisible for g = 001.

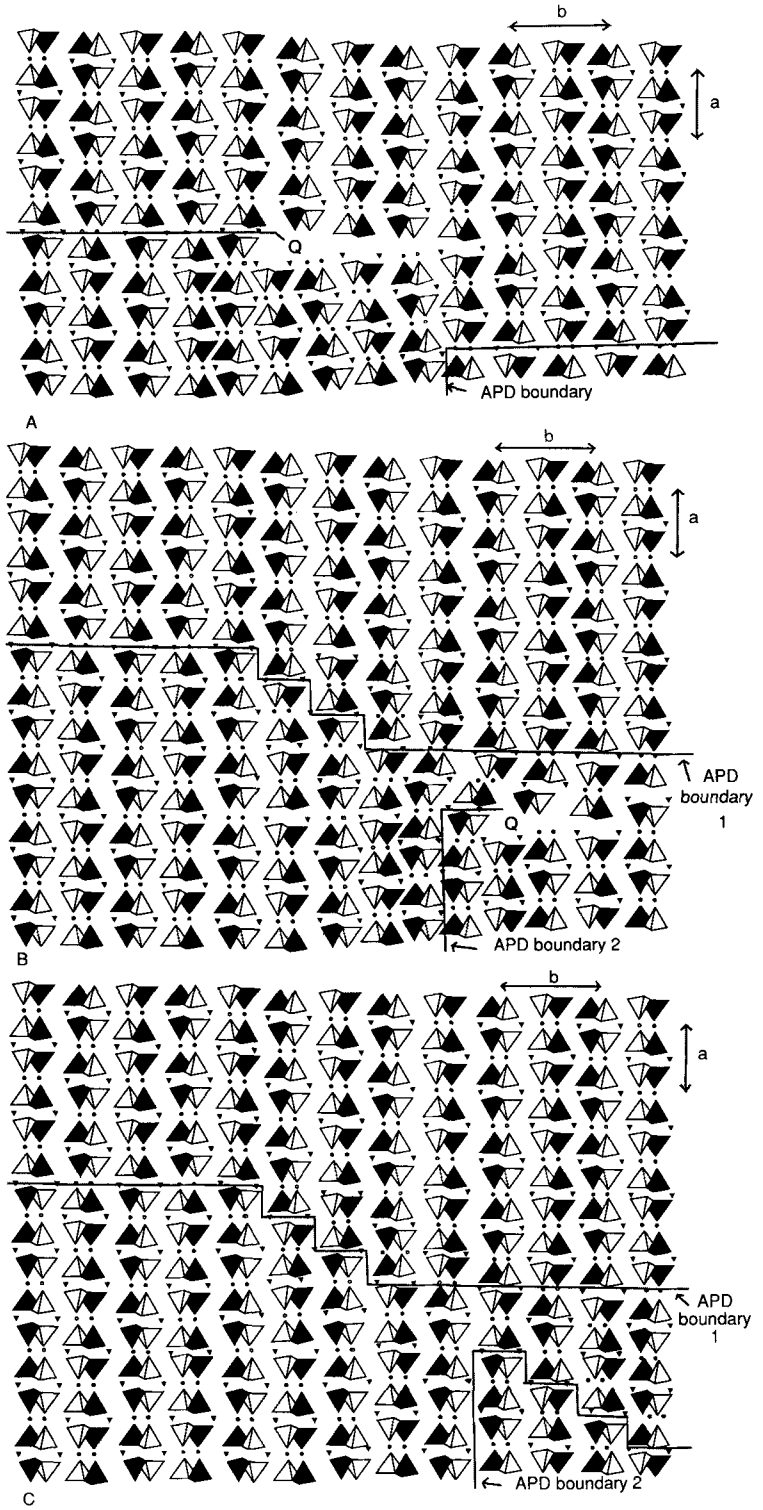
b
a
Q
APD boundary
A
b
a
APD
boundary
1
Q
APD boundary 2
B
b
a
APD
boundary
1
APD boundary 2
C

(1991), while a dislocation model illustrating the geometrical differences between 1/2<110> dislocations in the *C2/c* and *P2/n* crystal structures is given in Fig. 5. In the dislocation model of Fig. 5A and B we have chosen a simple dipole consisting of a positive (P) and a negative (Q) 1/2<110> edge dislocation. The dipole model was chosen because, in the case of an isolated 1/2<110> edge dislocation, a fault is introduced in the crystal. However, the geometry of the fault depends on the previous history of the dislocation, i.e. on whether it arrived at its position (P or Q) by climb or slip (Fig. 5B). As a consequence of this starting situation, the fault between dislocations P and Q in Fig. 5B is a crystallographic shear plane, since the displacement vector does not lie in the fault plane. Fig. 6C illustrates that a slipping (or climbing) 1/2<110> dislocation in the *P2/n* crystal structure will always drag the fault behind it. Comparison of the nature of the fault in Fig. 5B (R = 1/2<a+b>) with that of the APD boundary in Fig. 3 (R = 1/2<a+b>) shows that, despite their contrasting origins, both defects are identical in geometry.

Simulation studies

An example of the interaction between deformation-induced faults and the APD boundaries produced by cationic ordering in some naturally deformed omphacites from the Sesia Lanzo Zone is given in Fig. 6. It can be seen that the APD boundaries produced by cationic ordering end at 1/2<110> dislocations. This observation illustrates the interaction between the two processes. Furthermore, neighbouring 1/2<110> dislocations in the {110} tiltwall are connected by stacking faults (R = 1/2<110>).

A model of the effect of 1/2<110>{110} slip on the geometry of APD boundaries is illustrated in Figs. 7 and 8. In the model of Fig. 7 our starting situation (Fig. 7A) is the slipping 1/2<110> Q dislocation of Fig. 5B, but an APD boundary, produced by cationic ordering, is introduced in the bottom right side of the model. In Fig. 7B deformation has continued and the slipping 1/2<110> Q dislocation has passed the APD boundary. It can be seen that the APD boundary configuration is dramatically changed. This is due to the fact that, when the slipping 1/2<110> Q dislocation crosses the APD boundary, it 'cuts' the APD boundary in two pieces (APD boundary 1 and 2; Fig. 7B). Subsequently, APD boundary 1 attaches itself to the fault produced by the Q dislocation because both defects have the same displacement vector. APD boundary 2 attaches itself to the slipping Q dislocation and becomes subsequently dragged by it if deformation continues (Fig. 7C).

Fig. 8 illustrates the effect of APD boundary modification by dislocation glide at a smaller scale. For practical reasons we have used the simplified *I*-beam model of Papike *et al.* (1973). Also, the *P2/n* structure of omphacite in Fig. 8 is greatly oversimplified by the use of alternating black and white *I*-beam layers parallel to (010). These simplifications do not influence the results of our simulation studies. Fig. 8A shows the undeformed state with an APD boundary produced by cationic ordering. The NE–SW tracing line marks the slip plane of a future partial 1/2[110] dislocation [gliding in (110)]. In Fig. 8B this dislocation has passed through the crystal. Consequently the lower part of the crystal has been translated by 1/2 [-110] along (110). A dramatic change in the configuration of the antiphase domain boundary can easily be recognised. In Fig. 8C a 1/2[110] dislocation has passed, now gliding along (-110) and leaving behind a deformation-induced stacking fault. The nature of the latter, however, cannot be recognised from the image alone since both structures are identical in geometry and the associated partial dislocations are now outside the *P2/n* crystal.

In Figs. 7 and 8 we have illustrated the effect of one partial 1/2<110> dislocation on the configuration of one APD boundary. It is well known, however, that partial dislocations travel in pairs. Consequently one might argue that the original APD size configuration will be completely restored when the second partial dislocation has also passed. Our observations on the width of the deformation-induced faults between two partial 1/2<110> dislocations showed that its *minimum* width is *many* times the size of the small APDs. This observation is very important for the following reason. In Figs. 7 and 8 we introduced only one APD boundary. However, due to the fact that the deformation-induced fault width is many times the size of the small APDs, other APD

FIG. 7. Model of interaction between APD boundary and slipping partial 1/2<110> dislocation in *P2/n* omphacite. Projection parallel to (001). See text for further description. (A) Starting situation. (B) Situation after dislocation Q has crossed the APD boundary. (C) Dislocation Q has left the crystal.

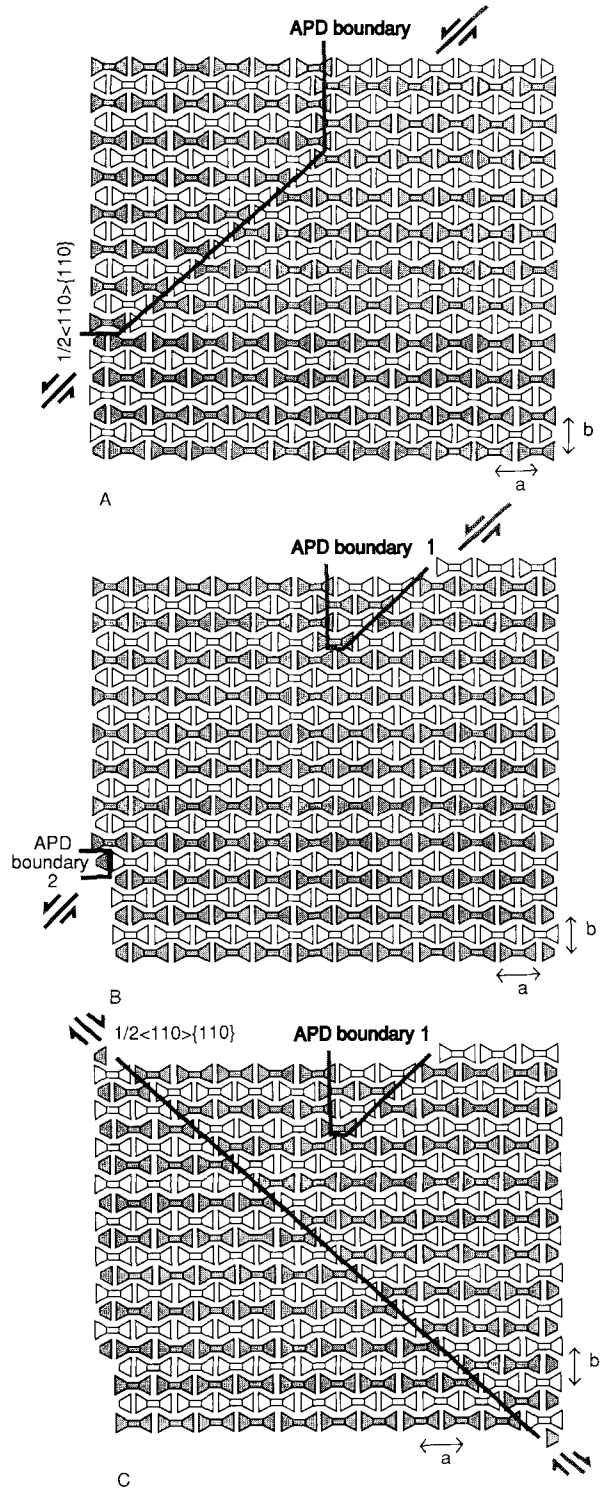
APD boundary
1/2<110>{110}
b
a
A
APD boundary 1
APD
boundary
2
b
a
B
1/2<110>{110}
APD boundary 1
b
a
C

boundaries will be present close to the deformation-induced faults. Imagine in Fig. 7A a second APD boundary at a distance of one tetrahedral layer away from the deformation-induced fault and running parallel to it. In such a situation the APD boundary will react with the deformation-induced fault to reduce the total length of the fault boundaries and so decrease the internal free energy of the crystal. We are currently unaware of such interactions in metallic or ceramic systems, but we regard it as being most likely, since the mobility of APD boundaries (and identical deformation-induced faults) have been documented by many authors (e.g. Carpenter, 1981*a*).

Discussion

From the foregoing it is concluded that APD sizes can be modified by dislocation slip and/or creep processes. However such processes alone cannot explain the observed bimodal APD size distribution. The biomodal size distribution results from a combination of the following processes: (1) APD formation by cationic ordering, followed by domain coarsening according to Carpenter's model (1981). If no deformation takes place, this gives rise to the observed, small, but relatively uniform APD sizes (250–350 Å). Corresponding temperature estimates are in reasonable agreement with other available thermometric methods (450–600 °C; Fig. 1). (2) If *P2/n* omphacite is deformed by deviatoric stresses during orogenesis, dislocation glide and/or creep processes will be superimposed on process 1. After deformation has ceased, the final APD sizes are produced by the operation of surface free-energy processes, leading to a reduction of the total length of APD boundaries. The ultimate APD size will vary from place to place, depending on the local deformation history. This results in the observed wide variation in coarse APD sizes. It is obvious, however, that the size of the coarse APDs cannot be used as a geothermometer. Detailed microstructural studies of internal deformation-induced phenomena (undulose extinction, subgrains, twinning etc.) combined with crystallographic fabric studies are therefore a prerequisite before APD sizes can be used for geothermometry (Carpenter, 1981). Emphasis on crystallographic fabric studies are especially important in high-temperature eclogites (garnet–omphacite-bearing rocks), since late-stage annealing processes can completely wipe out, on an optical scale, all internal deformation-induced defect structures in the omphacite. In such cases omphacite appears in thin section as optically strain-free crystals and the deformation history can only be recognised by crystallographic fabric and electron microscopic studies. If the orientation-distribution diagram of such omphacites reveals a clear crystallographic fabric defined by [001] parallel to *L* and [010] in a great circle distribution perpendicular to S and L, one should be careful with interpreting the APD sizes. Such crystallographic fabrics can only be explained by the operation of 1/2<110>{110}, {110}[001] and/or (100)[001] slip assisted by dislocation climb. The same is true for omphacite orientation-distribution diagrams defined by [010] perpendicular to S and [001] and [100] lying in a great circle distribution parallel to S. Although the latter cannot be explained by the operation of the presently known crystallographic slip systems in omphacite, a deformation origin is most likely. So far, however, no detailed electron microscopic studies have been performed to unravel the underlying dislocation substructures.

Another equally important consequence of the contrasting geometries of 1/2<110> dislocations in *C2/c* and *P2/n* omphacite crystals is that it may be possible to determine if the omphacite crystallised in the *C2/c* or *P2/n* stability field. If perfect deformation-induced 1/2<110> dislocations are present, the omphacite crystal must have crystallised and been deformed subsequently within the *C2/c* stability field. During cooling these perfect 1/2<110> dislocations become 'frozen-in' while the matrix omphacite transforms into the *P2/n* structure with associated APD formation. As long as the omphacite is not deformed, the perfect 1/2<110> dislocations will not affect the size distribution of these newly formed antiphase domains in the manner described above. However, the 1/2<110> dislocations still bear witness to the earlier high temperature *C2/c* nature of the omphacite. Alternatively, if the omphacite crystal is redeformed, after ordering takes place, migrat-

FIG. 8. Simplified model of *P2/n* omphacite illustrating the effect of two partial 1/2<110> dislocations on the original APD boundary geometry. Projection parallel to (001). See text for further descriptions. (A) Original APD boundary geometry. The future 1/2<110>{110} slip plane is indicated by the arrows. (B) The partial dislocation (b = 1/2 [-110]) has slipped through the crystal on (110). (C) Another dislocation (b = 1/2 [110]) has slipped through the crystal along (-110). Arrows mark slip plane/slip direction.

ing 1/2<110> dislocations will produce faults behind them. Such omphacite crystals thus contain dislocation substructures that bear witness to both deformation events. In the present case, for both metamorphic terrains, the compositions of the omphacites and the peak metamorphic temperatures indicate that omphacite growth took place within the *P2/n* stability field. The above mentioned T.E.M. observations on the contrasting properties of 1/2<110> dislocations are thus in agreement with the Champness (1973) metastable growth model of *C2/c* omphacites within the *P2/n* stability field. Cationic ordering was pre- and postdated by high temperature crystal plastic deformation.

Acknowledgements

H. L. M. v R. acknowledges receipt of the Louis Neel chair, sponsored by the Societé Lyonnaise de Banque, which allowed him to do this research as an associate professor at the Ecole Normale Supérieure de Lyon, Lyon, France. Also the manuscript benefitted from comments made by two anonymous reviewers.

References

Avé-Lallement, H. G. (1978) Experimental deformation of diopside and websterite. *Tectonophys.*, **48**, 1–27.

Boland, J. N. and Tullis, T. E. (1986) Deformation behavior of wet and dry clinopyroxenite in the brittle to ductile transition region. In *Mineral and rock deformation, lab. studies*, The Patterson Volume. Geoph. Monograph. Ser. Vol. 36 (B. E. Hobbs and H. G. Heard, eds.), 35–49. Am. Geoph. Union. Washington D.C.

Buatier, M. and Lardeaux, J. M. (1987) Deformation intracristalline de l'omphacite et du grenat en conditions de haute pression et basse température: exemple des éclogites de la zone Sesia–Lanzo (Alpes occidentales). *C.R. Acad. Sc. Paris*, **305**, 797–800.

——van Roermund, H. L. M., Drury, M., and Lardeaux, J. M. (1991) Deformation and recrystallisation mechanisms in naturally deformed omphacites from the Sesia-Lanzo zone. *Tectonophys.* In press.

Buseck, P. R., Nord, G. L., and Veblen, D. R. (1980) subsolidus phenomena in pyroxenes. In: Prewitt, C. T. (ed.), *Reviews in Mineralogy*, **7**. *Pyroxenes*. Min. Soc. Am., 117–204.

Caby, R., Kienast, J. R., and Saliot, P. (1978) Structure, metamorphisme et modèle d'évolution des Alpes occidentales. *Rev. Géogr. Phys. Géol. Dyn.*, **2**, 307–22.

Carpenter, M. A. (1981*a*) Omphacite microstructures as time-temperature indicators of blueschist and eclogite facies metamorphism. *Contrib. Mineral. Petrol.*, **78**, 441–51.

——1981*b*) Time-Temperature-Transformation (TTT) analysis of cation disordering in omphacite. Ibid. **78**, 433–40.

Carswell, D. A., Krogh, E. J., and Griffin, W. L. (1985) Norwegian orthopyroxene eclogites: calculated equilibrium conditions and petrogenetic implications. In Gee D. G. and Sturt B. A. (eds.), *The Caledonide Orogen in Scandinavia and Related Areas*. John Wiley, 823–42.

Champness, P. E. (1973) Speculation on an order–disorder transformation in omphacite. *Am. Mineral.*, **58**, 540–2.

Compagnoni, R., Dal Piaz, G. V., Hunziker, J. C., Gosso, G., Lombardo B., and Williams, P. F. (1977) The Sesia–Lanzo Zone, a slice of continental crust with alpine high-pressure–low-temperature assemblages in theWestern Italian Alps. *Rend. Soc. It. Min. Petrol.*, **33**, 281–334.

Dal Piaz, G. V. (1974) Le métamorphisme de haute pression et basse température dans l'évolution structurale du bassin ophiolitique alpino-apennique (1ère partie: considérations paléogéographiques). *Bull. Soc. Geol. It.*, **93**, 437–68.

Ellis, D. J. and Green, D. H. (1979) An experimental study of the effect of Ca upon garnet–clinopyroxene Fe–Mg exchange equilibria. *Contrib. Mineral. Petrol.*, **71**, 13–22.

Ingrin, J., Doukhan, N., and Doukhan, J. C. (1991) High-temperature deformation of diopside single crystals; part II: TEM investigation of the induced defect microstructures. Submitted to *J. Geophys. Research.*

Kienast, J. R. (1983) *Le métamorphisme de haute pression et basse température (éclogites et schistes bleus): données nouvelles sur la pétrologie de la croûte océanique subductée et des sédiments associés.* Thèse Dr. Sci., Université P. et M. Curie, Paris, 384 pp.

——Lombardo, B., Biino, G., and Pinardon, J. L. (1991) Petrology of very-high-pressure eclogitic rocks from the Brossasco–Isasca complex, Dora-Maira massif, Italian Western Alps. *J. Metamorphic Geol.*, **9**, 19–34.

Kirby, S. H. and Kronenberg, A. K. (1984) Deformation of clinopyroxenite: Evidence for a transition in flow mechanisms and semi-brittle behavior. *J. Geophys. Research*, **89**, 3177–92.

Koons, P. O. (1982) *An investigation of experimental and natural high-pressure assemblages from the Sesia Zone, Western Italian Alps, Italy.* PhD. thesis, ETH Zurich, 261 pp.

Lardeaux, J. M. and Spalla, M. I. (1991) From granulites to eclogites in the Sesia Lanzo zone (Italian Western Alps): a record of the opening and closure of the Piemonte ocean. *J. Metamorphic Geol.*, **9**, 1–25.

——Gosso, G., Kienast, J. R., and Lombardo, B. (1982) Relations entre le métamorphisme et la déformation dans la zone Sesia–Lanzo (Alpes occidentales) et le problème de l'éclogitisation de la croûte continentale. *Bull. Soc. Géol. France*, **24**, 793–800.

——Caron, J. M., Nisio, P., Pequignot, G., and Boudeulle, M. (1986). Microstructural criteria for reliable thermometry in low-temperature eclogites. *Lithos*, **19**, 187–203.

Lombardo, B., Nervo, R., Compagnoni, R., Messiga, B., Kienast, J. R., Mevel, C., Fiora, L., Piccardo, G. B., and Lanza, R. (1978) Observationi preliminari sulle ofioliti metamorfiche del Monviso (Alpi occidentali). *Rend. Soc. It. Mineral. Petrol.*, **34**, 253–305.

Nisio, P. (1985) *Les domaines d'antiphase des omphacites et la pétrologie des éclogites: contribution à l'étude de l'évolution tectonométamorphique du Monviso (Alpes italiennes occidentales)*. Thèse de doctorat, Univ. Lyon 1, 137 pp.

——Lardeaux, J. M., and Boudeulle, M. (1987) Évolutions tectonométamorphiques contrastées des éclogites dans le massif de Viso; consequences de la fragmentation de la croûte océanique lors de l'orogenese alpine. *C.R. Acad. Sc. Paris*, **304**, 355–60.

Papike, J. J., Prewitt, C. T., Sueno, S., and Cameron, M. (1973) Pyroxenes: comparisons of real and ideal structural topologies. *Z. Kristallogr.*, **138**, 254–73.

Phakey, P. P. and Ghose, S. (1973) Direct observation of anti-phase domain structure in omphacite. *Contrib. Mineral. Petrol.*, **39**, 239–45.

Philippot, P. (1988) Déformation et éclogitisation progressives d'une croûte océanique subductée; l'exemple du Monviso, Alpes occidentales. Contraintes cinématiques durant la collision alpine. *Doc. Traveaux Centre Géol. Géophys.*, **19**, 1–270. Montpellier, France.

——(1990) Opposite vergence of nappes and crustal extension in the French-Italian Alps. *Tectonics*, **9**, 1143–64.

Råheim, A. and Green, D. H. (1975) Experimental determinations of the temperature and pressure dependence of the Fe–Mg partition coefficient for coexisting garnet and clinopyroxene. *Contrib. Mineral. Petrol.*, **48**, 179–203.

Ratterson, P. and Jaoul, O. (1991) High-temperature deformation of diposide single crystals. Part 1. Steady state creep laws. Submitted to *J. Geophys. Research.*

Rossi, G. (1988) A review of the crystal-chemistry of clinopyroxenes in eclogites and other high-pressure rocks. In Smith D. C. (ed.), *Eclogites and eclogite-facies rocks*, 237–67.

——Smith, D. C., Ungaretti, L., and Domeneghetti, C. (1983) Crystal-chemistry and cation ordering in the system diopside-jadeite: a detailed study by crystal structure refinement. *Contrib. Mineral. Petrol.* **83**, 247–58.

Van Roermund, H. L. M. (1984) Omphacite microstructures from a Spanish eclogite. *Textures and microstructures*, **6**, 120–32.

——and Boland, J. N. (1981) The dislocation substructures of naturally deformed omphacites. *Tectonophys.*, **78**, 403–18.

Vuichard, J. P. (1989) La marge austroalpine durant la collision alpine: évolution tectonométamorphique de la zone Sesia–Lanzo. *Memoire et documents du C.A.E.S.S. n° 24, Rennes*, 1–160.

——and Ballèvre, M. (1986) Garnet–chloritoid equilibria in eclogitic pelitic rocks from the Sesia Zone (Western Alps): their bearing on phase relations in high-pressure metapelites. *J. Metamorphic Geol.*, **6**, 135–57.

[*Manuscript received 28 April 1991*]